Ligand dynamics in metal-organic frameworks

An experiment using the NCNR Disk Chopper Spectrometer

Wei Zhou, Nick Butch, and Craig Brown

Abstract

Time-of-flight neutron spectroscopy will be used to examine the high temperature dynamics of ligands in two metal-organic frameworks, $Mn[N(CN)_2]_2$.pyrazine (manganese dicyanimide pyrazine) and SIFSIX-1-Cu [1 = 4,4'-bipyridine; $Cu(bipy)_2(SiF_6)$]. This experiment illustrates the important technique known as quasielastic neutron scattering (QENS). We shall discuss all aspects of the experiment, from sample preparation and the choice of instrumental setup through to data treatment and interpretation of results.

I. Introduction

One of the major themes of solid state chemistry is the development of new molecular architectures with novel chemical and physical properties for applications such as chemical separation, catalysis and magnetic devices. One class of potentially useful materials is compounds consisting of metal ions or clusters linked together by organic ligands, widely known as "metal-organic frameworks" (MOFs). The bonding motifs and physical/chemical properties of these materials can be substantially altered by changing the metal and/or the organic ligands. For instance, $Zn[N(CN)_2]_2$ is a layered compound whereas its manganese analog, $Mn[N(CN)_2]_2$, is a three-dimensional "rutile" type material that is weakly ferromagnetic. Further modifications may be obtained by introducing ancillary π-conjugated ligands such as pyrazine (pyz), 4,4'-bipyridine and 2,2'-bipyridine. The molecular building blocks not only affect the spatial separation of the transition metal cations and the dimensionality of the crystal, but also modulate the super-exchange interactions. Of the $Mn[N(CN)_2]_2L$ type materials that have been studied, L = pyz is the only one that exhibits long-range antiferromagnetic order above 2 K.

Rietveld refinement of neutron powder diffraction (NPD) data for $Mn[N(CN)_2]_2$.pyz at 1.35 K reveals a three-dimensional antiferromagnetic ordering that occurs below T_N = 2.53(2) K, in which the magnetic unit cell is doubled along the a- and c-axes as compared with the nuclear cell (Figure 1). Crystallographic studies as a function of temperature
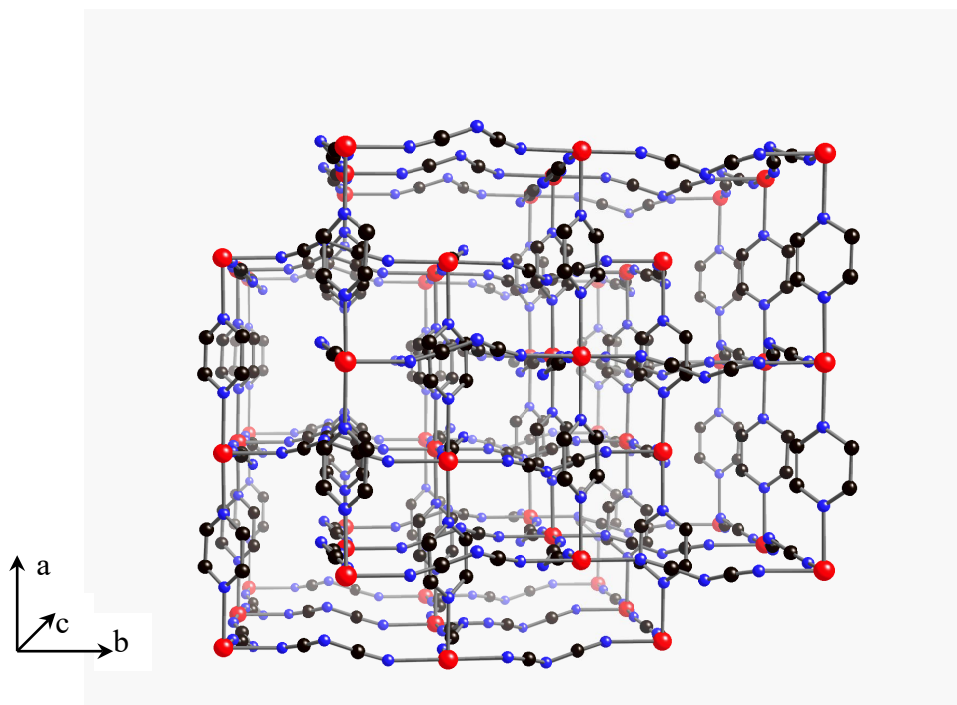

Figure 1. The low temperature crystal structure of $Mn[N(CN)_2]_2$.(pyz) is characterized by two interpenetrating ReO_3 type lattices. Manganese ions are depicted as large spheres, while carbon atoms are small black spheres and nitrogen atoms are small gray spheres. Hydrogen atoms are omitted for clarity.

confirm the existence of a monoclinic to orthorhombic phase transition at ~200 K. The transition is accompanied by an increase (with increasing temperature) in the diffuse scattering (figure 2), as well as a significant increase in the deuterium Debye-Waller factors. A further transition is evidenced by differential scanning calorimetry at ~408 K. The experiment with the Disk Chopper Spectrometer is designed to help us better understand what happens at the higher temperature transition.
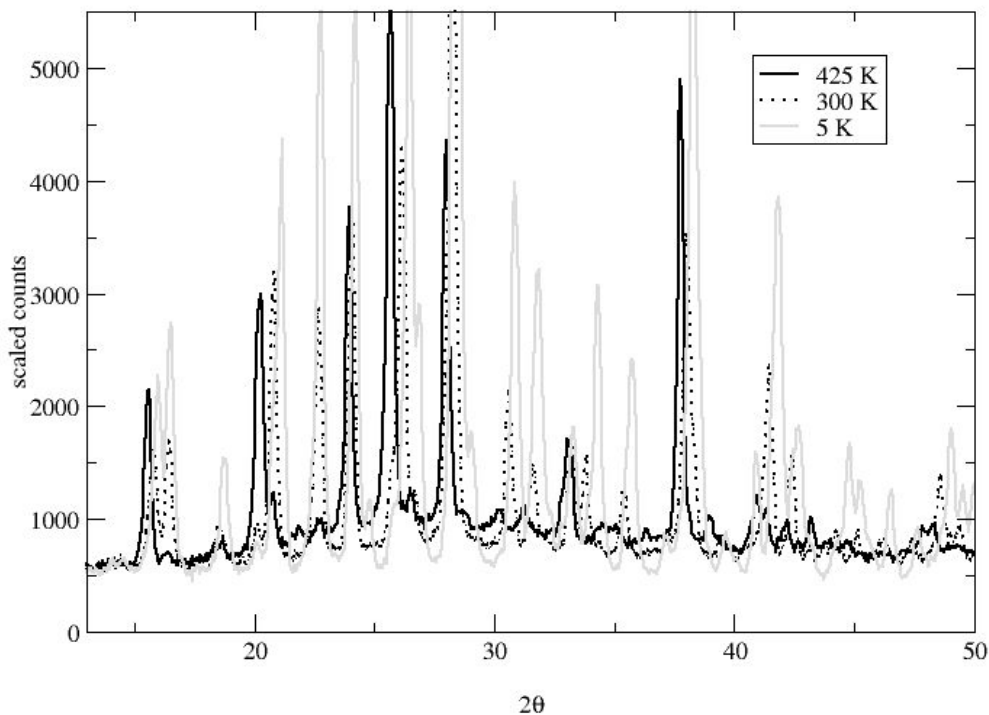

Figure 2. Selected portions of the neutron powder diffraction patterns of $Mn[N(CN)_2]_2.(pyz)$ taken with 1.54 Å neutrons at 5, 300 and 425 K, to highlight the increase in diffuse scattering with increasing temperature.

The neutron has several properties that enable scattering experiments to measure properties of materials that other techniques can measure with much less precision or not at all. Neutrons with wavelengths on the order of interatomic spacings also possess energies on the same order as those characteristic of phonons and intermolecular interactions; for example, a 1.8 Å neutron has an energy of ~25 meV (~200 cm^{-1}). This means that structural and temporal information can be measured simultaneously.

The reader is reminded that the scattering of neutrons is usually treated as the sum of two parts, known as _coherent_ and _incoherent_ scattering. To understand why such a separation is performed recall that the strength of the scattering from nuclei of the same element can

vary (and generally does vary) with spin and/or isotopic species. Hence when a neutron is scattered by a collection of nuclei the interference between the different scattered waves is normally neither complete nor completely absent. For this reason the _double differential cross section_ [$d^2\sigma/d\Omega d\omega$], which describes the probability that neutrons are scattered into solid angle $d\Omega$ and energy transfer window $d(\hbar\omega)$, is normally separated into two terms. The first term is the coherent part, which contains all of the interference effects such as Bragg scattering and small angle scattering. The second term is the incoherent scattering, which represents the scattering from individual nuclei and is approximately isotropic. For a single element [$d^2\sigma/d\Omega d\omega$] can be expressed as

$$\frac{d^2\sigma}{d\Omega d\omega} = \frac{1}{4\pi}\frac{k_f}{k_i}[\sigma_{coh}S(Q,\omega) + \sigma_{inc}S_{inc}(Q,\omega)] \qquad (1)$$

where k_i and k_f are the magnitudes of the initial and final neutron wavevectors, σ_{coh} and σ_{inc} are the coherent and incoherent scattering cross sections, and $S(Q,\omega)$ and $S_{inc}(Q,\omega)$ are the corresponding scattering functions which depend only on the momentum transfer $\hbar Q$ (or wave vector transfer Q) and the energy transfer $\hbar\omega$. (Note that in general Q is a vector but since we shall be working with a powder, which has no preferred orientation, all that need concern us in this experiment is the magnitude of the vector.) The most important incoherent scatterer is hydrogen for which σ_{inc} = 80 barns/atom whereas σ_{coh} is only 1.76 barns/atom (1 barn = 10^{-24}cm^2). Since the incoherent scattering cross section of hydrogen is much larger than those of almost all other nuclei, it is often reasonable (as a first approximation) to neglect the coherent scattering in systems that contain a relatively large fraction of hydrogen atoms.

> Can you explain the usefulness of deuteration, given that σ_{coh}(deuterium) and σ_{inc}(deuterium) are 5.6 barns/atom and 2 barns/atom, respectively?

Elastic neutron scattering is scattering with no change in neutron energy, i.e. with $\hbar\omega = 0$, and _inelastic neutron scattering_ is scattering with a change in neutron energy, i.e. with $\hbar\omega \neq 0$. On the other hand, _quasielastic neutron scattering_ (QENS) involves the Doppler-like broadening of otherwise elastically scattered neutrons due to reorientational or diffusive motions of atoms in the target material. Thus QENS is a special kind of inelastic neutron scattering. In this experiment we shall use quasielastic neutron scattering to obtain a physical description of the dynamics of the pyrazine ligand in Mn[N(CN)$_2$]$_2$.pyz at ~415 K, and to gain insights into the possible origin of the diffuse scattering observed in the powder diffraction data (figure 2).

We shall first describe the samples to be used for the experiment, and the equipment that will be used to bring samples to the desired measurement temperature. The next section gives a brief discussion of the spectrometer as well as matters to be considered in choosing the incident wavelength for this experiment. We then describe the reduction of the data to obtain the incoherent scattering function $S_{inc}(Q,\omega)$, and we follow with some words about the scattering that is expected for two possible models of the pyrazine ligand dynamics. This then sets the scene for the analysis and discussion of the experimentally measured scattering function.

In what follows we shall drop the subscript "inc" from $S_{inc}(Q,\omega)$ since the experiment is explicitly designed to measure the incoherent scattering function and the subscript is unnecessary.

II. The sample

Prior to the experiment several grams of the protonated sample (crystallographic density 1.636 g/cm^3) will have been loaded into a tall (10cm) annular aluminum cell (inner diameter 0.635 cm, outer diameter 1.27 cm), press sealed with lead wire. At the start of the experiment we shall mount the sample in a high temperature "displex" closed cycle helium refrigerator, and we shall heat it to 425 K, taking great care to ensure that its temperature never exceeds 435 K since it starts to decompose at about this temperature. Then, we shall collect data at the initial measurement temperature and at least one other temperature.

To reduce the data we will need results from a run with a deuterated sample (for reasons that will become apparent), from a normalization run using vanadium, and from a run with the beam closed.

All these runs will have been performed before the start of the summer school since it is a virtual school this time.

> Why do we typically use aluminum for sample containers and cryostat windows?
> What other materials might be used to seal sample containers?

III. The spectrometer

We shall be performing this experiment using the Disk Chopper Spectrometer (DCS), which is a so-called "direct geometry" (fixed incident energy) time-of-flight spectrometer. In this type of instrument (figure 3) bursts of monochromatic neutrons strike the sample at equally spaced times. The energies of the scattered neutrons are determined from their arrival times at the detectors, since we know when the pulses were created as well as the distances D_{PS} from the pulsing device to the sample and D_{SD} from the sample to the detectors. There are two ways to produce a monochromatic pulsed beam at a steady state neutron source. One method is to use a single crystal to monochromate the white beam and a mechanical "chopper" to pulse it; the other method is to use multiple choppers, such as the seven (!) choppers of the DCS.

A monochromatic pulsed beam of neutrons can in principle be created using two choppers. How does that work? Can you think why more than two choppers might be needed and/or desirable?
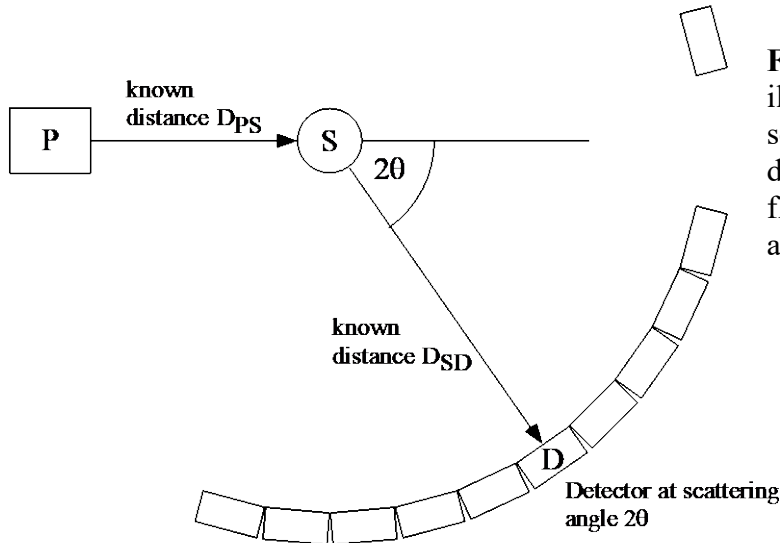

Figure 3. A schematic illustration of the scattering geometry for a direct geometry time-of-flight spectrometer such as the DCS.

Given the initial and final energies of the neutrons, E_i and E_f, the energy transfer $\hbar\omega = E_i - E_f$ is trivially obtained. Knowing the scattering angle 2θ we can also calculate the magnitude of the momentum transfer to the sample, $\hbar Q$:

$$(\hbar Q)^2 = 2m_n \left[E_i + E_f - 2\sqrt{E_i E_f} \cos 2\theta \right] \tag{2}$$

where m_n is the mass of the neutron. (This follows from the definition $\vec{Q} = \vec{k_i} - \vec{k_f}$ and the relationship between the magnitude of a neutron's wave vector, k, and its energy E: $E = h^2 k^2 / 2m_n$.)

The data acquisition system separately accumulates neutron counts for each of the 913 DCS detectors. Furthermore the time between pulses, T, is normally divided into 1000 time channels of equal width $\Delta t = 0.001T$ and each neutron event in a given detector is stored in one of these time channels according to its time of arrival at the detector. Thus the data acquisition system generates a two-dimensional array of counts I_{ij} as a function of detector index i and time channel index j. At the end of each run cycle the array is saved, along with other pertinent information, to the hard disk of the instrument computer.

At the DCS we shall first mount the sample environment on the sample table, taking care to position it correctly with respect to the incoming beam; to confirm the positioning of the sample we may use a TV camera system adapted for use with neutrons. We shall

6

bring the sample to its measurement temperature having connected the temperature controller to the instrument computer so that we can record the sample's temperature throughout the experiment.

An incident wavelength will then be selected, together with other instrument parameters such as the "master speed" of the choppers. The choice of wavelength is critical, and several factors must be considered. These include intensity at the sample (which peaks, remaining roughly constant, between ~2.5 and ~4.5 Å), the width of the elastic energy resolution function (which roughly varies as $1/\lambda^3$), the available Q range (which varies as $1/\lambda$), and concerns about "frame overlap" problems. A related consideration is the available range in sample energy gain (neutron energy loss).

> What is the maximum theoretical sample energy gain that can be measured when the incident energy is E_i, and how long would it take to measure the intensity of neutrons scattered with this change in energy?

Once the sample is at temperature, with the choppers phased, we will be ready to define the measurements to be performed through the night. We shall define a "sequence" consisting of several "runs" plus at least one change of sample temperature. We shall also define the individual runs. Each run is divided into a set of "cycles". At the end of each cycle the temperature is recorded, and the data are backed up to the disk. Having defined the runs, we shall start the overnight sequence of measurements. Next day we shall stop the measurements and start into the data reduction.

In the experimental runs we shall collect intensity histograms I_{ij} for the protonated version of the sample at at least two temperatures. Using previously acquired intensity histograms for the deuterated sample, for a vanadium sample and for a "dark count" run with the beam shutter closed, we shall reduce the data to obtain the double differential scattering cross section $[d^2\sigma/d\Omega d\omega]$ and the scattering function $S(Q,\omega)$.

IV. Data reduction

In this section we shall simply indicate some of the more important steps in the data reduction process. We shall go into greater detail in our discussions at the time that the data reduction takes place.

The measured scattering from the protonated sample comprises several components but we are only interested in one of these components: the incoherent quasielastic scattering from the hydrogen atoms. We shall therefore subtract the scattering from the deuterated sample, appropriately normalized, since to a good approximation it represents the elastic and quasielastic contributions from all the other atoms except hydrogen.

> What are some possible origins of the contributions to the scattering from atoms other than hydrogen?

Before doing this subtraction, we shall subtract a time independent background from each of the runs.

Where does the time independent background come from?

Neglecting effects such as self-shielding and multiple scattering the scattering in detector i and time channel j may be related to the corresponding double differential cross section $[d^2\sigma/d\Omega dt]_{ij}$ (note that this is per unit time, not energy) in the following fashion:

$$I_{ij} = \left[\frac{d^2\sigma}{d\Omega dt}\right]_{ij} \Delta\Omega\Delta t \cdot N_m \cdot \Phi_s \cdot \eta_{ij} \qquad (3)$$

where $\Delta\Omega$, the solid angle subtended by detector i, and Δt, the width of time channel j, are (for these measurements) presumed to be independent of i and j respectively, N_m is the number of sample molecules in the beam, Φ_s is the neutron flux at the sample, and η_{ij} is the efficiency of detector i for neutrons detected in time channel j.

Since we are not trying to extract an absolute cross section, we can neglect the multiplicative constants in the above equation, but we should not ignore the detector efficiency function η_{ij}. Since all of the detectors are to first order identical it is not unreasonable to treat η_{ij} as the product of two terms, a function η_{i0} which represents the efficiency of detector i for elastically scattered neutrons and a detector-independent function f_j that describes the energy dependence of the efficiency of the detectors. The correction for differences in detector response, i.e. the determination of η_{i0}, is performed using the results of a measurement with a vanadium sample.

Why do we use vanadium for this purpose?

The correction of the data for the energy dependence of the efficiency is achieved by calculation, knowing the various factors that affect the probability that a neutron is absorbed within a detector.

What are these factors?

To improve the statistics, recognizing that the incoherent scattering does not change rapidly with Q, we shall define several detector groups, each of which includes detectors within a specified range of angles. Since we are interested in the incoherent scattering, we shall exclude detectors that contain significant contributions from coherent Bragg scattering. The differential cross section $[d^2\sigma/d\Omega dt]$ for all detectors in a group will be summed and divided by the number of detectors in the group.

Having obtained a quantity proportional to $[d^2\sigma/d\Omega dt]$ we must now compute $[d^2\sigma/d\Omega d\omega]$ and finally $S(Q,\omega)$. Since a neutron's energy E is related to its time-of-flight t over a fixed distance as $E \propto t^{-2}$, it follows that $dE \propto t^{-3}dt$. Hence

$$\frac{d^2\sigma}{d\Omega d\omega} \propto \frac{d^2\sigma}{d\Omega dE_f} = \left[\frac{d^2\sigma}{d\Omega dt}\right]\left(\frac{dt}{dE_f}\right) \propto \left[\frac{d^2\sigma}{d\Omega dt}\right]t^3.$$

To obtain $S(Q,\omega)$ we simply divide by k_f (see eq. 1). Equivalently we multiply by another factor of t.

If a system in thermodynamic equilibrium can exist in a number of thermodynamic states and we consider two such states separated by an energy difference $\hbar\omega$, the probability that the system is in the lower energy state is greater by a factor $\exp(\hbar\omega/kT)$ than the probability that it is in the higher energy state. From this it can be shown that for systems in thermodynamic equilibrium the scattering function $S(Q,\omega)$ satisfies the so-called "detailed balance" relationship: $S(-Q,-\omega) = \exp(-\hbar\omega/kT)S(Q,\omega)$. Since we shall be fitting the data to a theoretical form that is symmetric in $\hbar\omega$ we shall first "symmetrize" the experimental $S(Q,\omega)$ by multiplying it by $\exp(-\hbar\omega/2kT)$.

> Is symmetrization of $S(Q,\omega)$ likely to be a large effect in this experiment?

Having reduced the experimental data to a symmetrized scattering function it is time to examine models that describe the motion of the hydrogen atoms in our sample, and corresponding predictions for the incoherent scattering function.

V. Theory

In this section we shall revert to using the subscript "inc" and we shall treat Q as a vector.

Most quasielastic experiments are performed on systems that predominantly scatter neutrons incoherently. The incoherent scattering function is the space and time Fourier transform of the *self-correlation function* $G_s(\vec{r},t)$ which (classically) represents the probability that a particle that was at the origin at time $t = 0$ is at position $\vec{r}$ at time t.

> Use a similar definition to relate the coherent scattering function to a (different) space-time correlation function. Why is it easier to formulate models of atomic motion using incoherent scattering?

A common way of expressing $S_{inc}(\vec{Q},\omega)$ is in terms of the *intermediate self scattering function* $I_s(\vec{Q},t)$, which is the space Fourier transform of $G_s(\vec{r},t)$:

$$S_{inc}(\vec{Q},\omega) = \frac{1}{2\pi}\int I_s(\vec{Q},t)e^{-i\omega t}dt \qquad (4)$$

An illustrative model for $G_s(\vec{r}, t)$ (though inappropriate in the context of the present experiment) is that of simple Brownian diffusion, where times of observation are much longer than typical times between collisions. Fick's Law governs this type of diffusion:

$$\frac{\partial}{\partial t} G_s(\vec{r}, t) = D\nabla^2 G_s(\vec{r}, t), \tag{5}$$

where D is the diffusion constant. A solution to this equation is given by a self-correlation function of the form

$$G_s(\vec{r}, t) = \frac{\exp(-r^2 / 4Dt)}{(4\pi Dt)^{3/2}}, \tag{6}$$

the space Fourier transform of which is

$$I_s(\vec{Q}, t) = \exp(-Q^2 Dt). \tag{7}$$

Since this represents an exponential decay in time, the time Fourier transform yields a Lorentzian lineshape:

$$S_{inc}(\vec{Q}, \omega) = \frac{1}{\pi}\left[\frac{DQ^2}{(DQ^2)^2 + \omega^2}\right] \tag{8}$$

that is centered at zero energy transfer and has a full width at half maximum height (FWHM), Γ, given by

$$\Gamma = 2DQ^2. \tag{9}$$

We shall now consider a quite different (and much more appropriate) model, representing the diffusional motion of hydrogen atoms among equivalent sites. As before we need only consider the motion of a single hydrogen atom. We consider the case of jump diffusion on a finite number of sites that lie on a circle. The rate equation that describes the real time motion of an atom is

$$\frac{df_i(t)}{dt} = -\frac{1}{\tau} f_i(t) + \frac{1}{\tau} \sum_{j \neq i} f_j(t), \tag{10}$$

where $f_i(t)$ is the probability that a particular atom is at site i at time t, τ is the time between jumps, and the sum is taken over all sites from which the molecule can jump directly to site i. Considering the particularly simple case of a proton undergoing jumps between just two equivalent sites, the rate equations are

$$\frac{df_1(t)}{dt} = -\frac{1}{\tau} f_1(t) + \frac{1}{\tau} f_2(t) \quad \text{and} \quad \frac{df_2(t)}{dt} = \frac{1}{\tau} f_1(t) - \frac{1}{\tau} f_2(t). \tag{11}$$

Hence

$$\frac{d}{dt}\left[f_1(t) + f_2(t)\right] = 0 \tag{12}$$

which also follows from the fact that $f_1(t) + f_2(t) = 1$ (by definition). Assuming the particle is at site 1 initially (i.e. at t=0), the solutions are

$$f_1 = \frac{1}{2}\left(1+\exp\frac{-2t}{\tau}\right) \quad \text{and} \quad f_2 = \frac{1}{2}\left(1-\exp\frac{-2t}{\tau}\right) \tag{13}$$

Writing

$$G_s(\vec{r},t) = f_1(t)\delta(\vec{r}) + f_2(t)\delta(\vec{r}-\vec{R}) \tag{14}$$

where $\vec{R}$ is the vector between the two positions, $I_s(\vec{Q},t)$ can be evaluated as

$$I_s(\vec{Q},t) = \frac{1}{2}\left(1+\cos\left[\vec{Q}.\vec{R}\right]\right) + \frac{1}{2}\left(1-\cos\left[\vec{Q}.\vec{R}\right]\right)\exp\frac{-2t}{\tau}. \tag{15}$$

From this equation we see that the Fourier transform of the first term, which is time-independent, gives a delta function in energy whereas the second term has an exponential time dependence that leads to a Lorentzian component in the quasielastic scattering. The result of performing a three-dimensional powder average and the final Fourier transform is as follows:

$$S_{inc}(Q,\omega) = \frac{1}{2}\left(1+\frac{\sin[QR]}{QR}\right)\delta(\omega) + \frac{1}{2}\left(1-\frac{\sin[QR]}{QR}\right)\frac{1}{\pi}\left(\frac{2\tau}{4+\tau^2\omega^2}\right). \tag{16}$$

This is the basic equation that you will use to fit your data in the next section.

> What is the FWHM of the Lorentzian component, and how does it compare with the that of the Lorentzian that we obtained for long range translational diffusion?

The fractional intensity of the elastic component as a function of momentum transfer is termed the _elastic incoherent structure factor_ (EISF). From the EISF one can learn something about the microscopic geometry of the motion. In figure 4 we illustrate the expected EISF for the uniaxial two-fold jump model described above and for the case where the number of jump sites is so large that it approximates uniaxial rotational
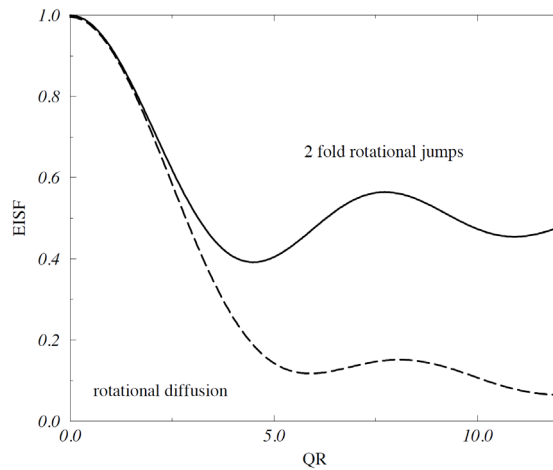

Figure 4. The elastic incoherent structure factor for uniaxial two-fold rotational diffusion (solid line) and for uniaxial rotational diffusion (dashed line) as a function of QR.

diffusion. In principle, it is possible to tell if a particle is undergoing rotational jumps or continuous diffusion on this basis alone. Practical limitations on maximum measurable Q values restrict this distinction to 6-fold jumps or less.

> What is the asymptotic value of the EISF for the two-fold jump model as Q→∞? What is it for rotational diffusion? What would you expect the scattering function to look like for a system where three-fold jumps occur among equivalent sites?

VI. Data analysis

Having reduced the data to the symmetrized form of the experimental scattering function $S(Q,\omega)$, Q representing the average value of the elastic scattering vector for the detectors in each group, the next step is to fit the data to a model. We suggest that you try fitting each Q group to the two-fold jump model described in the previous section (i.e. an elastic delta function and a broader Lorentzian). In an actual experiment the scattering function is broadened with the instrumental resolution function so the model function must be numerically convoluted with the instrumental resolution function.

Having fitted the experimental data to the two-fold jump model, the next step is to make plots of the Lorentzian line width and of the EISF as functions of Q. It is then instructive to fit the EISF to its functional form (according to the model), in order to extract the jump distance R.

> (1) With what can the jump distance R be compared, and how does it compare?
> (2) What can you learn from the Q dependence of the widths of the Lorentzian components?
> (3) Can you explain how the diffraction data (figure 2) and the QENS data (from your experiment) relate to one another?

VII. Concluding remarks

In section V we discussed scattering functions that correspond to very simple models of diffusive motion. The situation is more complicated when a system displays more than one type of diffusive motion. If the various motions are uncoupled, the intermediate scattering function is a product of the individual intermediate scattering functions so that the scattering function is a convolution of the scattering functions for the individual motions. The situation simplifies considerably if the motions occur on very different time scales. Motions that are much slower than the time scale represented by the instrumental resolution show up as elastic scattering. On the other hand, motions that are much faster

give rise to an essentially flat background. Different instruments, with different dynamical windows and different resolution capabilities, are needed to observe such motions. For example, motions that are too slow to see using the DCS may well show up if the sample is put on the backscattering spectrometer. Conversely motions that are fast by DCS standards can usefully be studied using the FANS facility.

VIII. General references

- G.E. Bacon, "*Neutron Diffraction*", Clarendon Press, Oxford (1975).

- M. Bée, "*Quasielastic Neutron Scattering*", Adam Hilger, Bristol (1988)

- R. Hempelmann, "*Quasielastic Neutron Scattering and Solid State Diffusion*", Clarendon Press, Oxford (2000).

- S.W. Lovesey, "*Theory of Thermal Neutron Scattering from Condensed Matter*", Clarendon Press, Oxford (1987).

- G.L. Squires, "*Introduction to the Theory of Thermal Neutron Scattering*", Cambridge University Press (1978), republished by Dover (1996).

- J.R.D. Copley and J.C. Cook, "*The Disk Chopper Spectrometer at NIST: a new instrument for quasielastic neutron scattering studies*", Chem. Phys., 292, 477 (2003).

- C.M. Brown and J.L. Manson, "*Solid State Ligand Dynamics in Interpenetrating $Mn[N(CN)_2]_2(pyrazine)$*", J. Am. Chem. Soc., 124, 12600 (2002).

Appendix A. Instrument Characteristics for the Disk Chopper Spectrometer

(https://www.nist.gov/ncnr/dcs-disk-chopper-spectrometer)

The white beam from the cold neutron source is cleaned of high energy neutron and gamma ray contamination using an "optical filter". This is basically a bent guide which ensures that there is no line of sight from the source to points beyond the local shutter. A cooled graphite filter removes short wavelength (~0.5 Å) neutrons that remain in the beam, permitting measurements at wavelengths down to roughly 1.5 Å.

A clean, pulsed, monochromatic neutron beam is produced using seven disk choppers. Chopper speeds may be varied from 1200 to 20000 rpm. The pulsing and monochromating choppers have three slots of different widths. In principle this permits three choices of intensity and resolution at a given wavelength and master chopper speed.

The measured intensity at the sample is reproduced below. Red and blue points correspond to measurements using different chopper slot widths.
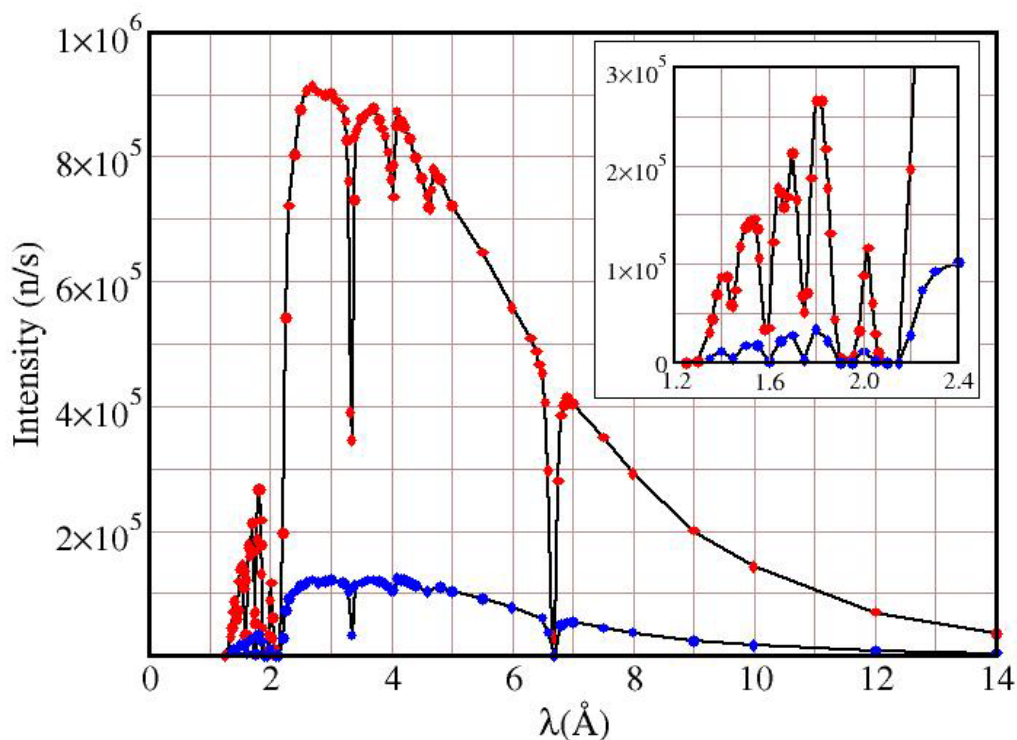
Why are there dips in the measured flux at wavelengths near 3.335 and 6.67 Å? What's going on around 2 Å?

The resolution of the instrument is approximately triangular and essentially independent of beam height (10 cm) but depends on the width of the beam. Hence samples should ideally be tall and thin rather than short and fat.

The measured elastic energy resolution, for the same choices of chopper slot width as in the intensity plot above, is shown in the figure below. Lines represent fits to the measurements.
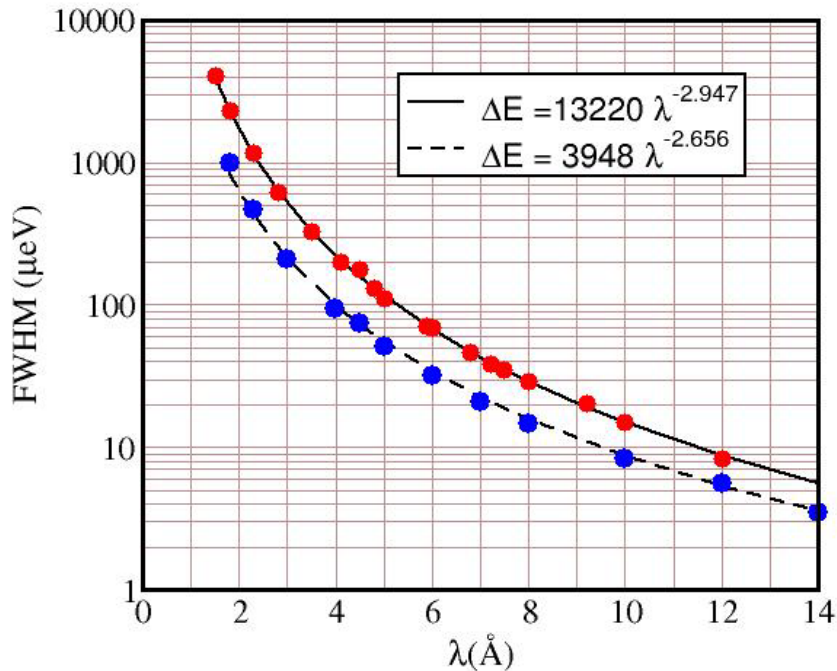
An oscillating radial collimator, inside radius 200 mm, outside radius 300 mm, blade separation 2°, is used to reduce the scattering from sample environment structures.

> Can you explain how the radial collimator works, and why it is oscillated?

There are 913 six atmosphere ^{3}He detectors covering an essentially continuous solid angle of ~0.65 steradians and arranged in three banks:
- Middle bank detector scattering angles range from -30° to -5° and from +5° to +140°
- Upper and lower bank angles range from -30° to -10° and from +10° to +140°

The flight distance from sample to detectors is 4010 mm. The flight chamber is purged with argon.

> Why is the flight chamber purged with argon?

Appendix B. Possible Experiments on the Disk Chopper Spectrometer

Phenomena that can be investigated include:
- Translational and rotational diffusion processes, where scattering experiments provide information about time scales, length scales and geometrical constraints; the ability to access a wide range of wave vector transfers, with good energy resolution, is key to the success of such investigations
- Low energy vibrational and magnetic excitations and densities of states
- Tunneling phenomena
- Low Q powder diffraction

Research areas include:
- **Chemistry ---** e.g. clathrates, molecular crystals, fullerenes
- **Polymers ---** bound polymers, glass phenomenon, confinement effects
- **Biological systems ---** protein folding, protein preservation, water dynamics in membranes
- **Physics ---** adsorbate dynamics in microporous/mesoporous systems (MOFs, zeolites, clays etc.) and in confined geometries, metal-hydrogen systems, glasses, magnetic systems
- **Materials ---** negative thermal expansion materials, low conductivity materials, hydration of cement, carbon nanotubes, proton conductors, metal hydrides

Appendix C. Some useful properties and relationships

Neutron properties

Mass: 1.660×10^{-24} g
Electric charge: 0
Spin: ½
Magnetic moment: -1.913 nuclear magnetons

Exact relationships

$$\lambda = \frac{h}{mv} \qquad E = \frac{1}{2}mv^2 \qquad k = \frac{2\pi}{\lambda}$$

Approximate relationships

$$E[meV] = \frac{81.8}{(\lambda[\text{Å}])^2}; \quad v[mm/\mu s] = \frac{3.956}{\lambda[\text{Å}]}; \quad E[meV] = 2.07(k[\text{Å}^{-1}])^2; \quad 1 \text{ meV}=8.1 \text{ cm}^{-1}$$

Relevant cross sections (in barns/atom) (V.F. Sears, Neutron News **3** (3) 26 (1992)

	σ_{coh}	σ_{inc}	σ_{abs}
H	1.7568(10)	80.26(6)	0.3326(7)
D	5.592(7)	2.05(3)	0.000519(7)
C	5.550(2)	0.001(4)	0.00350(7)
N	11.01(5)	0.50(12)	1.90(3)
Mn	1.75(2)	0.40(2)	13.3(2)

For most elements the absorption cross section σ_{abs} is proportional to $1/v$ where v is the neutron velocity: note that $m_n v = h/\lambda$. The values given in the table are for 2200 m/s neutrons.

Appendix D. Spin Incoherence

The strength of the scattering of a neutron by a nucleus, i.e. the neutron scattering length, depends on the spin of the compound nucleus. For an isotope with nuclear spin I the combined "nucleus + neutron" spin, I', has two possible values, $I^+ = I+1/2$ and $I^- = I-1/2$, with which we associate two possible scattering lengths b^+ and b^-. Each of the possible values of the combined spin has $2I'+1$ possible spin states, i.e. $2(I+1/2)+1 = 2I+2$ and $2(I-1/2) +1 = 2I$ states respectively, for a total of $4I+2$ spin states.

If the neutron and nuclear spins are randomly orientated, all states are equally probable, and the probabilities of the combined + and - spin states are $p^+ = (I+1)/(2I+1)$ and $p^- = I/(2I+1)$ respectively.

The mean scattering length, <b>, and the mean of the scattering length squared, <b²>,

$$\langle b \rangle = p^+ b^+ + p^- b^- \quad \text{and} \quad \langle b^2 \rangle = p^+ (b^+)^2 + p^- (b^-)^2$$

are used to calculate the coherent and incoherent bound cross sections. These cross sections are defined as follows:

$$\sigma_{coh} = 4\pi \langle b \rangle^2 \quad \text{and} \quad \sigma_{inc} = 4\pi \left(\langle b^2 \rangle - \langle b \rangle^2 \right).$$

Working through the numbers for hydrogen and deuterium is instructive. The relevant scattering lengths for hydrogen are $b^+ = 1.086 \times 10^{-12}$ cm and $b^- = -4.751 \times 10^{-12}$ cm, whereas the values for deuterium are $b^+ = 0.951 \times 10^{-12}$ cm and $b^- = 0.095 \times 10^{-12}$ cm.

Appendix E. Pyrazine Geometry

Below, is a pictorial representation of the pyrazine as refined from powder diffraction data taken at low temperature. Selected inter-atomic distances between nitrogen (blue), carbon (gray) and hydrogens (white) are defined by the arrows and are given in Ångstroms.